

Supporting Information

Fabrication of Ordered Bi-Metallic Array with Superstructure of Gold Micro-Rings via Templated-Self-Assembly Procedure and its SERS Application

Zhangyu Yin,^{a,b} Yuchen Zhou,^c Pengcheng Cui,^{a,b} Jinhua Liao,^{a,b} Miriam H.

*Rafailovich^c and Wei Sun^{*a,b}*

^aDepartment of Materials Science and Engineering, School of Materials Science and Chemical Engineering, Ningbo University, Ningbo, 315211, China

^bState Key Laboratory Base of Novel Functional Materials and Preparation Science, School of Materials Science and Chemical Engineering, Ningbo University, Ningbo 315211, China

^cDepartment of Materials Science and Chemical Engineering, Stony Brook University, Stony Brook, New York 11794, United States

Corresponding Author

*E-mail: sunwei@nbu.edu.cn.

Experimental

Materials

Polystyrene (PS) ($M_w=1.92\times 10^5$), didodecylamine (DDA) and 4-aminothiophenol (4-ATP) were purchased from Sigam-Aldrich. Ascorbic acid (AA) and 3-aminopropyltriethoxysilane (APTES) were purchased from Shanghai Energy Chemical Co., Ltd. 3-Mercaptopropyltrimethoxysilane (MPTS) was purchased from Shanghai Aladdin Bio-Chem Technology Co., Ltd. Octadecyltrichlorosilane (OTS) was purchased from Macklin Reagent Co., Ltd. Methanol, tetrachloroauric (III) acid tetrahydrate ($\text{HAuCl}_4\cdot 4\text{H}_2\text{O}$) and polyvinylpyrrolidone (PVP) were purchased from Sinopharm Chemical Reagent Co., Ltd. Chloroform (CHCl_3) and toluene were purchased from Hangzhou Gaojing Fine Chemical Industry Co., Ltd.. Deionized (DI) water ($18.2 \text{ M}\Omega \text{ cm}^{-1}$) was provided by a lab-water system (HK Super PW). All the chemicals were used without further purification.

Preparation of perforated breath figure (BF) films

Firstly, the glass substrates ($5 \times 8 \text{ mm}$) were pre-treated with piranha solution ($\text{H}_2\text{SO}_4 : \text{H}_2\text{O}_2 = 70 : 30, \text{ V/V}$) at $75 \text{ }^\circ\text{C}$ for 30 min to modify the surface of glass with hydroxyl group, then cleaned with DI water and nitrogen dried before placing them in a sealed glass container. The BF process was operated in the container filled with saturated water vapor, and different concentrations of PS solutions in CHCl_3 with DDA (0.9 mg/mL) were prepared and cast onto glass substrates to make BF films. The perforated BF films were prepared by casting $6 \text{ }\mu\text{L}$ of polymer solution onto the glass substrate with a micro-syringe under room temperature. After complete solvent evaporation, the obtained film was removed into a desiccator for further drying.

Preparation of bi-metallic arrays

Silicon wafer ($5 \times 8 \text{ mm}$) was treated with piranha solution at $90 \text{ }^\circ\text{C}$ for 30 min, and cleaned with DI water and nitrogen dried. Different silanes were dissolved in toluene with the concentration of $5 \times 10^{-3} \text{ mol/L}$, and the cleaned wafer was immersed into the silane solution for certain amount of time (2h for MPTS and APTES, several different lengths of time were tried for OTS). After the completion of immersion, the wafer was cleaned in toluene, ethanol and DI water by ultrasonic cleaning, and

nitrogen dried for the next step.

The as-prepared perforated film was soaked in methanol for 5 min and then lift off the glass substrate, transferred onto the silicon wafer. After that, the perforated film on the silicon wafer was coated with a layer of Pt nanoparticles (NPs) via magnetron sputtering deposition. Then, the polymeric film was dissolved away by immersing the substrate into CHCl_3 . The sample was then soaked in 0.5 mL of fresh aqueous solution containing AA (0.1 mol/L) and PVP (0.01 g/mL). 20 μL of aqueous solution of $\text{HAuCl}_4 \cdot 4\text{H}_2\text{O}$ (0.1 mol/L in DI water) was injected into the immersion solution consecutively at the speed of 0.2 $\mu\text{L/s}$. After 30 s of reaction, the sample was taken out with plastic forceps, then cleaned with DI water and nitrogen dried.

Characterization

The deposition of Pt NPs was completed by using a magnetron sputtering system (MSP-1S, Japan SHINKKU VD). The surface and cross-sectional structures of the different samples from different fabrication steps were characterized with field emission scanning electron microscopes (FE-SEM, JEOL JSM-7600F and FEI Nova Nano SEM 650). The elemental mapping of energy dispersive X-ray spectroscopy (EDX) measurements were performed on the JEOL JSM-7600F thermal FE-SEM equipped with Oxford Instruments' energy dispersive spectroscopy (EDS) and wavelength dispersive spectroscopy (WDS) detectors. Acceleration voltage of 15 kV was used to probe well into the substrate. Atomic force microscope (AFM) images were taken on Bruker Dimension Icon using contact mode. The chemical states of the MPTS modified silicon substrate before and after the Pt sputtering were measured by X-ray photoelectron spectroscopy (XPS, K-Alpha+, Thermo Scientific). And all the binding energies were calibrated by setting the C (1s) at 284.8 eV. Wettability of all the silicon wafers treated with piranha solution and silanes were measured by a contact angle meter (DSA100, Krüss) at room temperature.

For the surface-enhanced Raman scattering (SERS) measurement, the as-prepared bi-metallic array samples were soaked in 4-ATP aqueous solutions for 6 h, rinsed with DI water and dried under room temperature. Raman spectra were recorded by a microscopic confocal Raman spectrometer (Renishaw PLC) employing a 633 nm

laser beam. The spectra were obtained by focusing the laser spot (diameter of 1 μm) on the samples using a 50 \times objective lens, and the signals were collected repeatedly for 3 times within 2 s. Raman measurements for different samples were carried out under identical experimental conditions (laser wavelength and power, microscope objective/lenses, etc).

Supporting figures

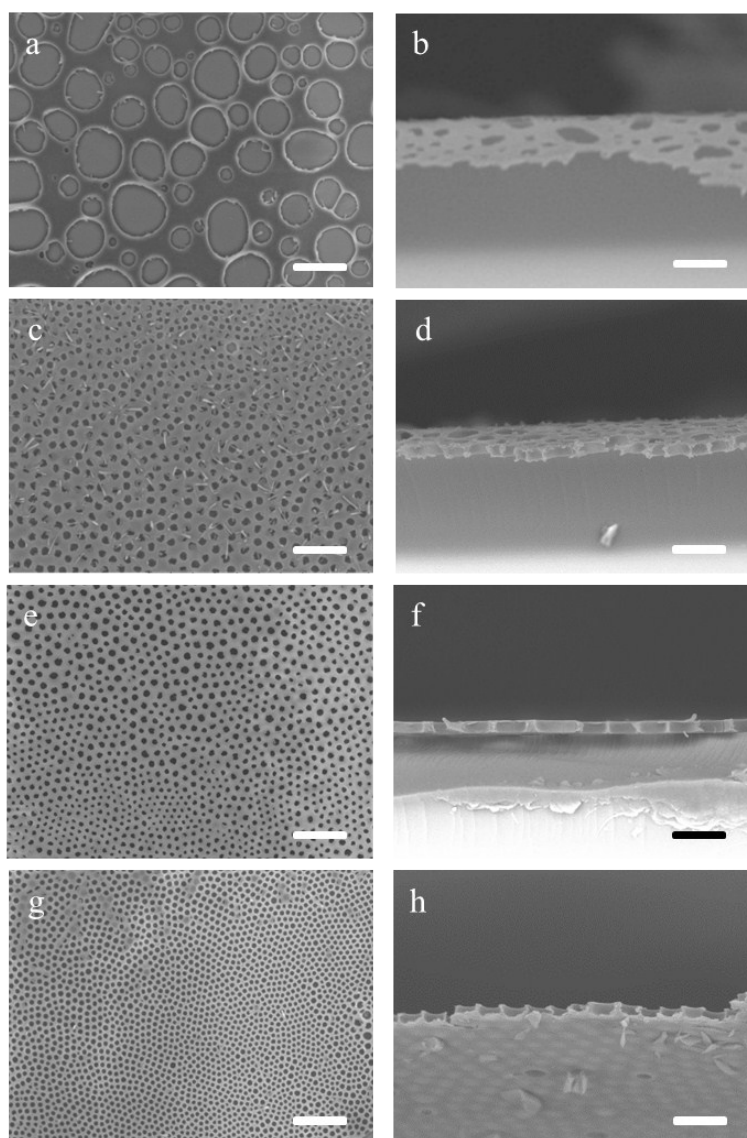


Fig. S1. SEM images showing the top view (left column) and cross-sectional view (right column) of the porous BF films on glass substrate prepared by casting the PS/ CHCl_3 solutions mixed with amphiphilic surfactant of DDA. Different concentrations of PS were adopted in the film making: (a-b) 2.5; (c-d) 5; (e-f) 7.5; (g-h) 10 mg mL^{-1} . Scale bar: (a, c, e, g) 20 μm ; (b, d, f, h) 5 μm .

Discussion on S1: Fig. S1 shows the surface and cross-sectional morphologies of the PS films prepared from the BF casting solutions with different polymer concentration. Highly ordered and through-pore structures were obtained under the condition of medium concentration (Fig. S1c-f). Irregular porous perforated film was obtained

under the condition of low concentration (Fig. S1a,b). While for the case of high concentration, as shown in Fig. S1g,h, rather thin bottom layer of polymer was formed, resulting in dead-end pore arrays. It could be concluded that the perforation of the BF film could be achieved by simply casting dilute polymer solution. In order to produce perforated porous film with fine BF patterns, suitable concentration of the polymer solution had to be chosen. If the cast solution became too thin, due to the incapability of the thin liquid layer of polymer in stabilizing the orderly arranged water droplets, the resultant pore arrays became disordered even with the assistance of fair amount of amphiphilic surfactant. While once the polymer solution became too thick, the growth of the water droplets would be suppressed by the polymer layer which stabilized the templating droplets during the BF process. Hence, it became difficult for the droplets to rupture the polymer solution film, resulting in the failure to complete the perforation.

The resultant perforated BF pores were not quite regularly arranged as the classic honeycomb-structured BF pattern. Hexagonal regularity of the pores was limited in local areas on the surface (Fig. S1e). Such irregularity was attributed to the fact that rather dilute polymer solution was used to prepare the film in order to achieve the perforation of the templating water droplets. The low concentration of the casting solution could not provide sufficient stabilization effect for achieving fine arrangement of the templating water droplets. While when the concentration was high enough to produce large area of hexagonal arrangement, the perforation could not be achieved (as shown in Fig. S1g,h). So, the lack of regularity for the BF films in our work was a “trade-off” to achieve perforation of the BF pores by performing regular BF procedure.

All the BF masks were prepared on the glass substrates before transferred to the treated silicon wafers for subsequent masking step. The BF mask was not made directly on the wafer, because the difference in the surface chemistry and hence wettability (see Fig. S7) between the differently treated wafers would significantly affect the formation of the perforated BF pores. For most cases of the treated substrates, the perforation could not even be achieved. Therefore, we have to prepare

the BF masks on the glass substrate first to make sure of the reproducibility of the perforated pores and transferred the masks onto the treated wafers afterwards. In that way, we could make arrays of Pt discs with consistent morphologies on the differently treated substrates for studying their influence on the growth of Au superstructures.

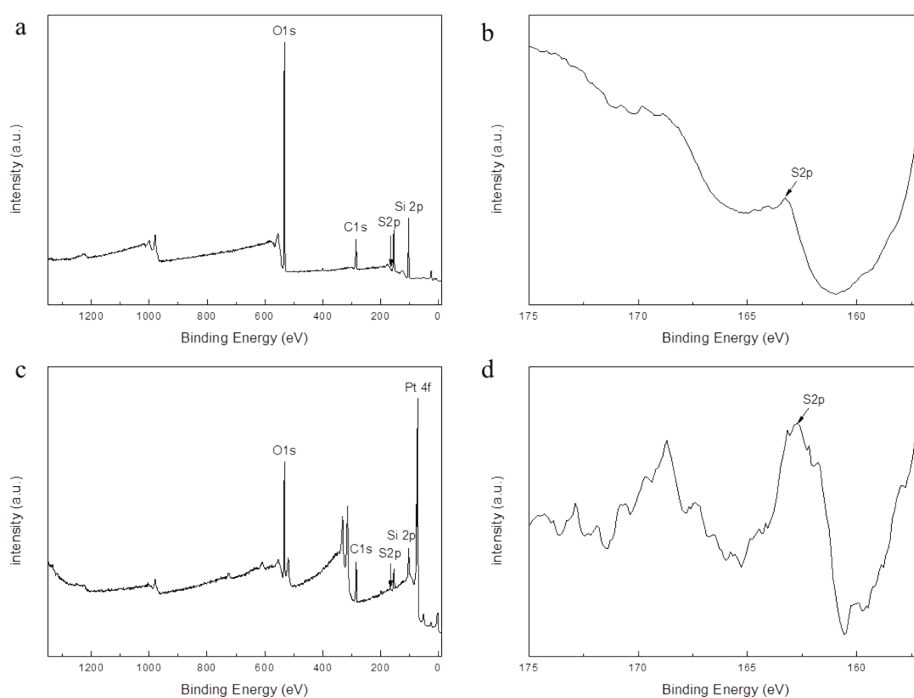


Fig. S2. XPS survey spectrum (a) and S 2p peak (b) of MPTS-coated silicon substrate before the Pt sputtering. XPS survey spectrum (c) and S 2p peak (d) of MPTS-coated silicon substrate after the Pt sputtering.

Discussion on S2: In the high-resolution scan of XPS spectra acquired from the MPTS-coated silicon substrate, as shown in Fig. S2b, the S 2p peak located at 163.1 eV is the characteristic of sulphur in mercapto group ($-SH$).^{1,2} While for the sample after the ion sputtering of Pt and the removal of the polymeric template, the S 2p peak is still present and located at 162.7 eV (Fig. S2d), which can qualitatively account for the validity of the thiolated substrate after the BF masking process. It could be concluded that the sulfhydryl group was successfully attached onto the substrate before Pt sputtering, and remained intact in the regions between the Pt discs after the sputtering.

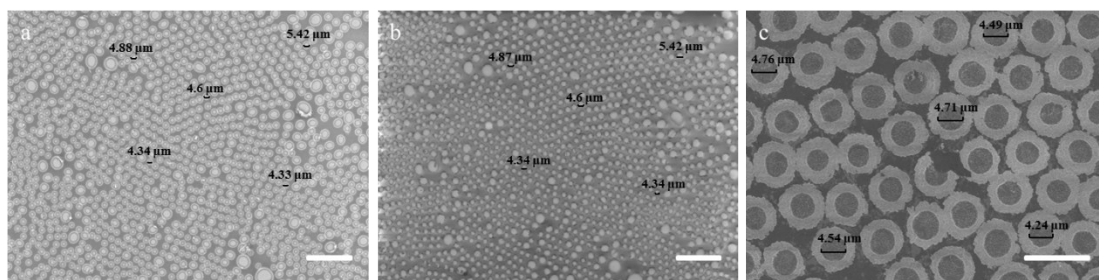


Fig. S3. SEM images of the same thiolated substrate in different steps of the TSA procedure: (a) the as-prepared perforated BF mask; (b) the Pt discs obtained after the Pt sputtering and the removal of BF mask; (c) the bi-metallic array obtained after the deposition of the Au NPs. Scale bars: (a,b) 20 μm ; (c) 10 μm .

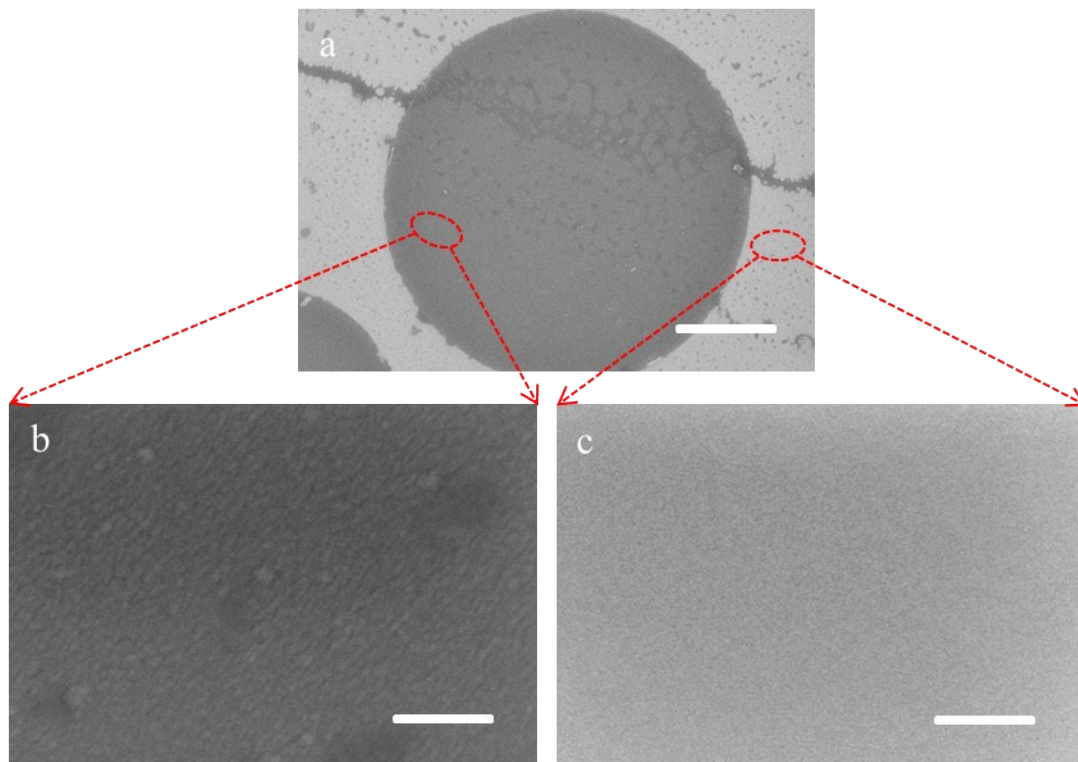


Fig. S4. (a) SEM image of single Pt disc after the BF masking process. The detailed SEM images show surface morphology of the (b) Pt disc and (c) the substrate regions between the discs. Scale bars: (a) 2 μm ; (b, c) 100 nm.

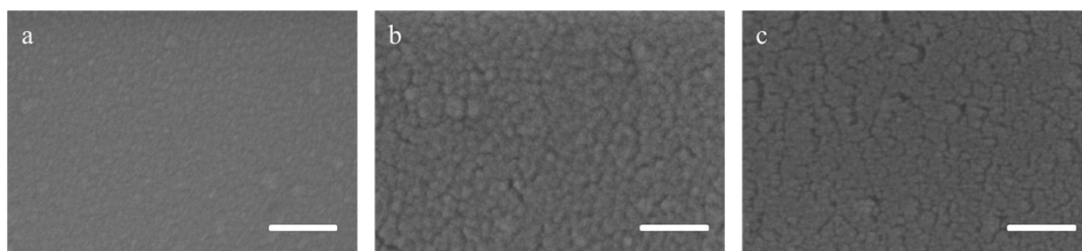


Fig. S5. SEM images of the Pt discs fabricated under different sputtering time: (a) 1 min; (b) 2 min; (c) 3 min. Scale bars: 100 nm.

Discussion on S4 & S5: Fig. S4c,d show the detailed surface morphology of the disc and the regions other than the discs respectively. One could see that compared with the rough morphology, composed of densely deposited NPs, of the Pt disc, the in-between regions showed no particular roughness. Such high selectivity of the NP deposition together with the high replication accuracy reflected the fact that the masking effect of the perforated BF film was satisfying. Moreover, the Pt NPs within the disc grew larger with increased sputtering time (Fig. S5), showing that the fine control on the disc morphology could be achieved.

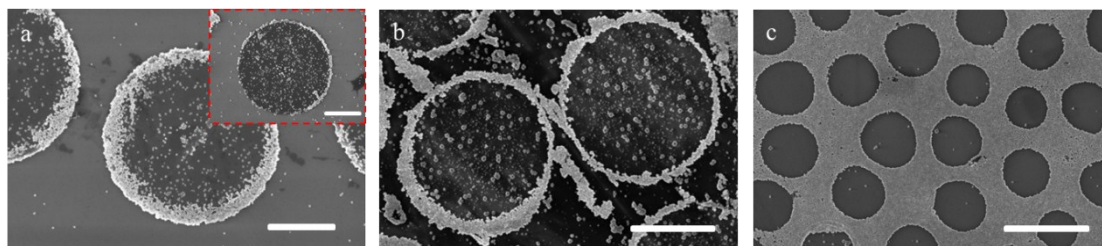


Fig. S6. SEM images of the bi-metallic arrays prepared on silicon wafers functionalized with different end groups: (a) hydroxyl group; (b) amino group and (c) alkyl group. Scale bars: (a) 2 μm ; (b,c) 5 μm ; (a inner) 500 nm.

Discussion on S6: To further evaluate the influential factors upon the formation of the Au superstructure, more types of the surface groups on the substrate were tested for their influence in the growth of the Au NPs onto the Pt arrays. By using the substrates modified by amino and hydroxyl group to collect the deposited Au NPs, the ring-like morphology of the obtained superstructure were also achieved (Fig. S6a,b). Comparing with the case of thiolated substrate, the Au rings formed on the substrates with amino and hydroxyl group showed thinner walls. There were even incomplete rings formed on the hydroxyl-functionalized wafer (Fig. S6a inner). It could be attributed to the fact that Au is attractive to the sulfhydryl group via bonding connection (ref. 19,20 of the manuscript), which is much stronger than the connection between hydroxyl or amino group and the deposited Au NPs. In the case of thiolated substrate, the Au NPs could be more extensively distributed onto the substrate, resulting in much thicker Au rings than the ones on the substrates with the other two end groups. All the three adopted end groups rendered the substrate surface hydrophilic (see the contact angle results in Fig. S7a-c). For comparison, hydrophobic alkyl group was also used. As a result, rather distinct superstructure of the deposited Au NPs appeared. The particles grew into a continuous honeycomb-structured network structure, covering all the void substrate between the Pt discs (Fig. S6c). The allocation of the deposited particles showed high priority towards the exposed substrate over the Pt discs.

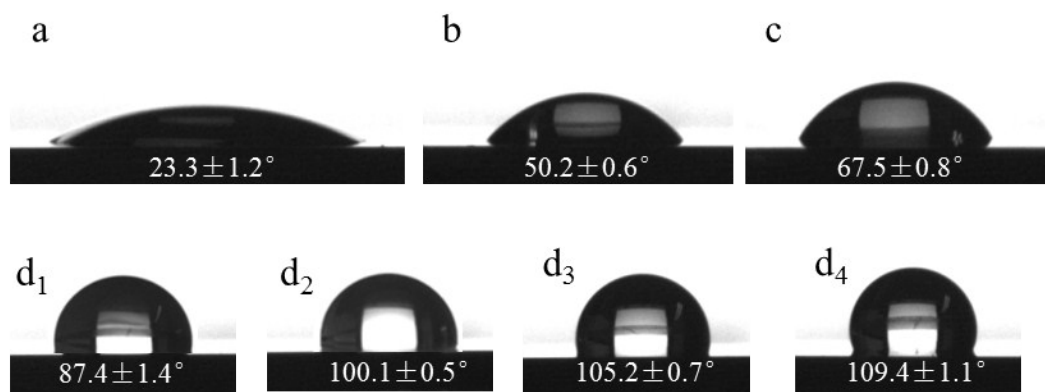


Fig. S7. Water contact angle images and values of silicon wafers treated with piranha solution (a) and chemically modified with silanes with different end groups: (b) amino group; (c) sulfhydryl group; (d) alkyl group with different treating time: (d₁) 10 s; (d₂) 60 s; (d₃) 300 s; (d₄) 900 s.

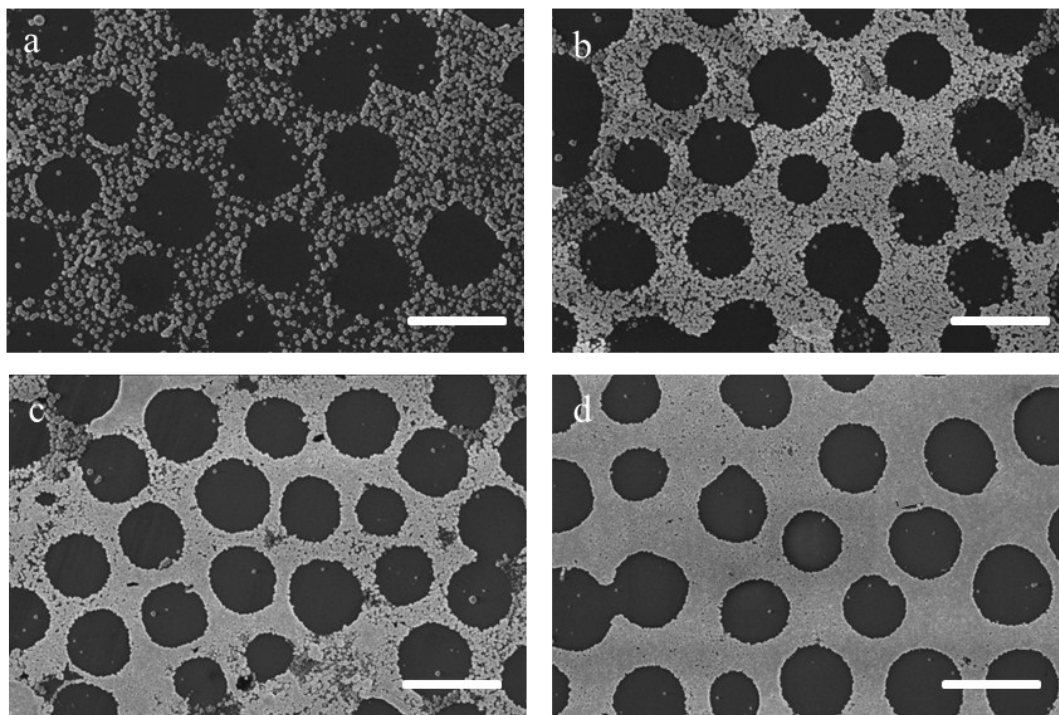


Fig. S8. SEM images of the bi-metallic arrays prepared on silicon wafers modified with alkyl group. The silicon substrate was treated for different amount of time beforehand: (a) 10 s; (b) 60 s; (c) 300 s; (d) 900 s. Scale bars: 5 μm .

Discussion on S8: Interestingly, when we tuned the degrees of the hydrophobicity of the alkyl-binding substrates by varying the silane treating time (Fig. S7d₁₋₄), the coverage of the deposition of Au NPs changed accordingly (Fig. S8). With the increased value of contact angles of the alkylated substrate, hence being more hydrophobic, the assembling superstructure of Au NPs grew from being sparsely clustered to densely packed.

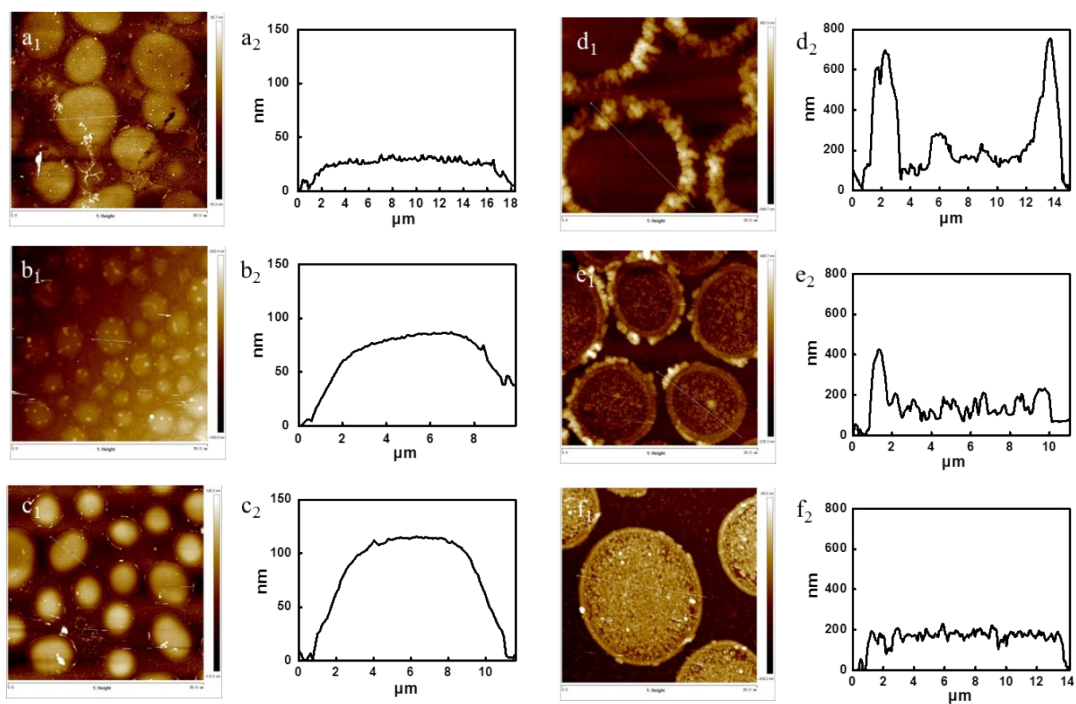


Fig. S9. AFM height images and sectional view along the lines in the images of the Pt discs before the deposition of Au NPs (a-c) and bi-metallic arrays (d-f) with different Pt sputtering time: (a,d) 1 min; (b,e) 2 min; (c,f) 3 min.

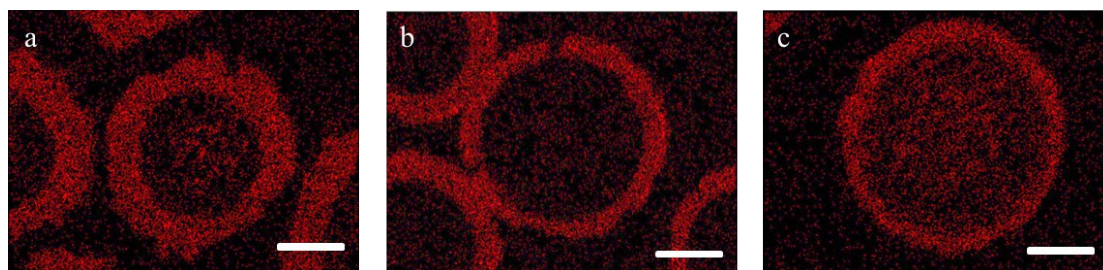


Fig. S10. Au EDX mapping images of the bi-metallic arrays with different Pt sputtering time: (a) 1 min; (b) 2 min; (c) 3 min. Scale bars: 2 μm .

Discussion on S9 & S10: The AFM cross-sectional profiles of the rings, grown from discs with different sputtering time (Fig. S9d-f), confirmed the fact of the descending ring walls and elevating discs inside the rings. And by analyzing together with the cross-sectional profiles of the Pt discs before the Au deposition (Fig. S9a-c), one could conclude that the accumulation of the Au NPs as well as the thickening of the disc from prolonged sputtering contributed for the increased lateral roughness inside the rings. The build-up of the NPs inside the rings with increased sputtering time was also confirmed to be from the reduction of Au by examining the elemental mapping of EDX in Fig. S10.

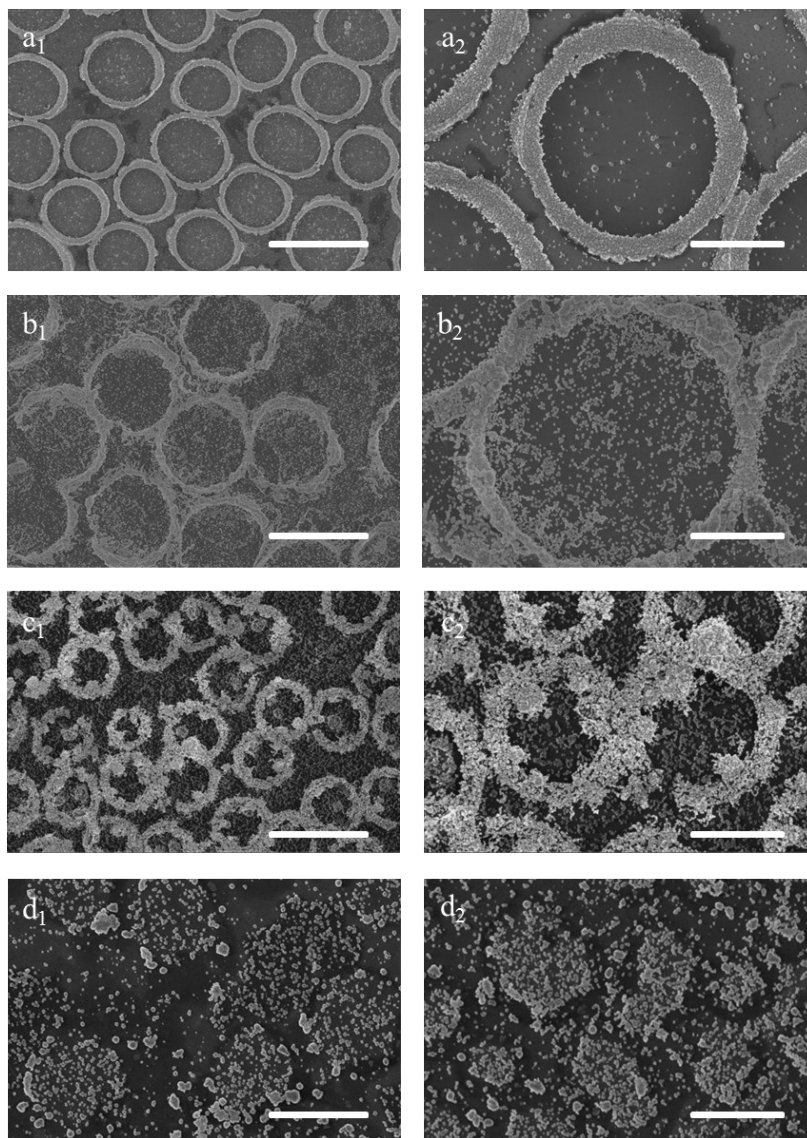


Fig. S11. SEM images of the bi-metallic arrays fabricated by soaking thiolated substrates with Pt discs in the solutions with different concentrations of HAuCl₄. The concentration of AA and PVP in the solutions remained to be 0.1 M and 0.01 g/mL, respectively. Concentrations of HAuCl₄: (a) 0.1 M; (b) 0.2 M; (c) 0.4 M; (d) 0.8 M. Scale bar: (a₁-d₁) 5 μm; (a₂-d₂) 2 μm.

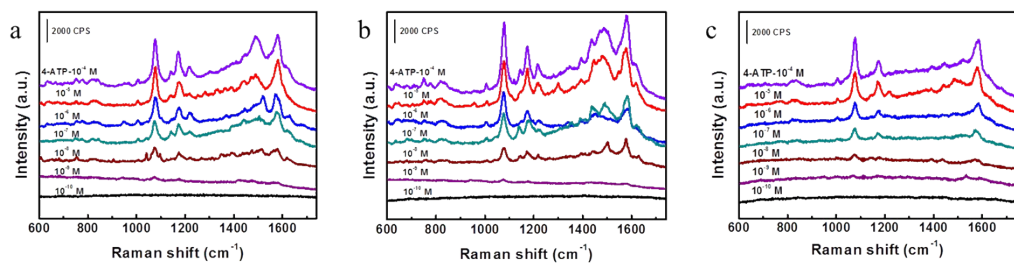


Fig. S12. SERS spectra of 4-ATP with different concentration adsorbed on (a) sample S2, (b) sample S3 and (c) honeycomb-structured sample as shown in Fig. S6c.

Calculation of SERS enhancement factor

The surface enhancement factor (EF) was calculated according to the following expression:^{3,4}

$$EF = (I_{\text{SERS}}/I_{\text{bulk}}) \times (N_{\text{bulk}}/N_{\text{ads}})$$

where I_{SERS} is the intensity of a specific band in the SERS spectrum of 4-ATP and I_{bulk} is the intensity of the same band in the Raman spectrum from the solid sample. N_{bulk} is the number of molecules of the bulk 4-ATP while N_{ads} is the number of molecules adsorbed on the substrate.

$$N_{\text{bulk}} = N_{\text{av}} \times \rho \times V_{\text{laser}}/M_{4\text{-ATP}}$$

where N_{AV} is Avogadro number (6.02×10^{23} molecules/mol), V_{laser} is laser excitation volume, ρ is the density of 4-ATP molecules (~ 1.18 g/cm³), $M_{4\text{-ATP}}$ is molar mass of 4-ATP molecules (125.19 g/mol). The spot diameter of the laser beam was ~ 1 μm and its penetration depth was also ~ 2 μm . Then, the total number of bulk molecules would be 8.91×10^9 .

$$N_{\text{ads}} = N_{\text{d}} \times A_{\text{N}} \times A_{\text{laser}}/\sigma$$

where N_{d} is the number density of the NPs, A_{laser} is the area of the focal laser spot with a diameter of 1 μm , A_{N} is the area of the NPs, and σ is the surface area occupied by an adsorbed 4-ATP molecule. According to the report by Kim,⁵ each 4-ATP molecule occupies ~ 0.20 nm² on full coverage of Au, indicating that σ can be adopted as ~ 0.20 nm²/molecule. N_{d} and A_{N} can be obtained from the SEM images. Then, the number of 4-ATP molecules illuminated by the laser light would be 6.3×10^5 .

With I_{SERS} and I_{bulk} measured at 1078 cm⁻¹, the ratio of $I_{\text{SERS}}/I_{\text{bulk}}$ of sample S3 was determined to be 29.84, and the EF of 4-ATP adsorbed on bimetallic array is about 4.22×10^5 .

REFERENCES

- 1 F. Sinapi, S. Deroubaix, C. Pirlot, J. Delhalle and Z. Mekhalif, *Electrochimi. Acta*, 2004, **49**, 2987-2996.
- 2 Y. Qi and X. H. Cheng, *J. Exp. Nanosci.*, 2015, **10**, 189-198.
- 3 P. H. Camargo, L. Au, M. Rycenga, W. Li and Y. Xia, *Chem Phys Lett*, 2010, **484**, 304-308.
- 4 E. C. Le Ru, E. Blackie, M. Meyer and P. G. Etchegoin, *J. Phys. Chem. C*, 2007, **111**, 13794-13803.
- 5 K. Kim and J. K. Yoon, *J. Phys. Chem. B*, 2005, **109**, 20731-20736.